Journal of Thermal Analysis and Calorimetry
https://doi.org/10.1007/s10973-026-15468-6

Tripalmitin-driven phase segregation in multicomponent fats

Julia Seilert[1] · Michael Rappolt[2] · Georg Dol[3] · Eckhard Flöter[1]

Received: 17 February 2025 / Accepted: 16 March 2026

Abstract

This contribution reviews the recrystallization of high-melting components in PO (PO)-based fat blends monitored by differential scanning calorimetry (DSC) and time- and temperature-resolved small- and wide-angle X-ray scattering (SAXS/WAXS) in four different case studies. Different temperature-time profiles, including annealing, were applied to investigate the crystallization kinetics with focus on mixed crystal formation (co-crystallization) and its potential for being controlled. The main focus was hereby to capture phase segregation events during melting. These segregation effects are caused by true recrystallization from either the melt or melt-mediated polymorphic transition of the tripalmitin (PPP)-rich high-melting fraction. The first case study illustrates the formation of mixed crystals by step-wise crystallization and evaluation of the subsequent melting DSC curve. By applying low heating rates, the evolution of the observed melting points combined with information on lamellar spacings revealed a time-dependent formation of the medium-melting fraction. The second case study discusses the effects and interplay of heating rate, crystallization temperature, and partial melting on the phase segregation in PO crystallization. The third case study focuses on PPP as driver for phase segregation in a palm-based commercial hardstock (PCM). Fourth, the same PCM was subjected to different crystallization routines including annealing to modify the mixed crystals formed. Deduced from SAXS/WAXS observations, annealing during the cooling step proved greatly aiding the formation of a mixed crystal, which would withstand phase segregation of PPP during the melting.

Graphical abstract

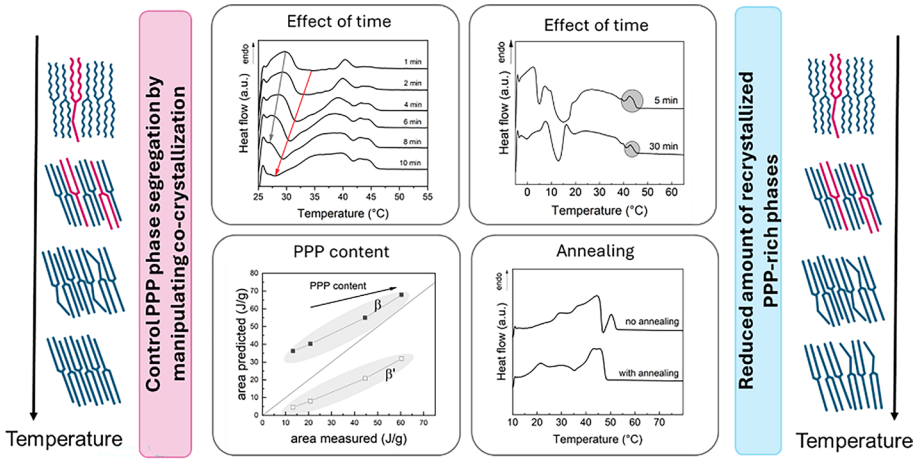

Keywords Differential scanning calorimetry · Phase segregation · Polymorphic transition · Crystallization · TAGs

Extended author information available on the last page of the article

Published online: 12 April 2026

Introduction

Differential scanning calorimetry (DSC) is a valuable tool to investigate the thermal behavior of multicomponent fats. Triacylglycerol (TAG) crystallization can take place in multiple steps depending on the fat blend's composition and applied process. In general, the mixing behavior of TAGs plays a crucial role. Molecular similarities and general tendencies toward fast or slow nucleation determine phenomena such as mixed crystal formation, co-crystallization, separate crystallization, and formation of molecular compounds [1–3]. Further, the process parameters (e.g., cooling rate, crystallization temperature) [4] affect the homogeneity of crystalline phases. Further, changes in the composition within a crystal is limited due to low diffusion rates in the solid phase. [1, 5, 6]

Crystallization events like polymorphic transition and sequential crystallization can overlap rendering it difficult assigning specific events to the corresponding peaks in a melting curve. Moreover, DSC data are prone to superposition of kinetic effects, either intrinsic to the sample or due to experimental execution, e.g., scan rate [7]. By applying different temperature-time profiles it is possible to disentangle the influence of the techniques' parameters (i.e., thermal lag and instrument equilibration determined by scan rate) and true sample response affected by polymorphism [8, 9] and sequential or co-crystallization of different fractions depending on the blend's composition [10–12]. Foubert et al. [13] suggested the so-called 'stop-and-return' method for DSC. The method offers an indirect approach to follow the amount of crystallized fat over time. The procedure involves interrupting the isothermal crystallization at different times. The subsequent heating scan is analyzed by integrating the melting profiles with the area as measure for the amount of crystallized fat. This analysis can only be performed, if no recrystallization takes place during the melting scan, i.e., a high heating rate must be applied [7].

Another technique to study fat crystallization is X-ray scattering. The polymorphic form can be determined from reflections in the wide-angle region (WAXS). The lamellar stacking is derived from reflections in the small-angle region (SAXS) [14–16]. The structural diversity of TAGs causes variation of the plane repeat distances. A combination of DSC and X-ray analysis allows determining the crystallization pathways in view of polymorphic transition and phase segregation. This was successfully applied to study the crystallization of palm oil (PO) (fractions) in recent years [17–19].

The crystallization of PO is of special interest given its many-faceted use in the food industry due to its naturally occurring high amount of saturated monoacid TAGs like tripalmitin (PPP), 5–7%, and up to 35–40% mono-unsaturated TAGs such as 1,3-dipalmitoyl-2-oleoyl-*sn*-glycerol and 1,2-dipalmitoyl-3-oleoyl-*sn*-glycerol (abbreviated as POP and PPO) [20]. It is also a prominent example for multiple-step crystallization, which is relied on in PO fractionation to yield high-quality stearin and olein. PO is known to exhibit a complex crystallization behavior hampering the fractionation process, including phenomena such as mixed crystal formation, co-crystallization, and the formation of molecular compounds [21]. For example, PPP shows the tendency to co-crystallize with PPO and POP and molecular compounds thereof [22–25]. This not only complicates the separation process to reach high-purity fractions but also its replacement as structuring fat. For both, the control of the crystallization behavior is crucial.

The complex crystallization of PO was subject of numerous calorimetric and rheological studies that postulate that a two-step process observed at low temperatures is caused by, first, the formation of an α polymorph that undergoes a transition into a β' polymorph [26–30]. The α phase nucleates from the solution consisting of TAGs of PO's high-melting fractions. The transition was reported to be enhanced by shear [30–32] and affected by the applied cooling rate [18, 33]. A study by West and Rousseau reported that the crystallization of PO's higher melting fraction containing PPP and POP/PPO is largely driven by PPP [34]. Trisaturated TAGs engage in selective co-crystallization in the presence of mono-unsaturated TAGs [35].

Some research focused on the effect of different TAG fractions on the crystallization kinetics in fats. For example, Cisneros et al. reported that the low-melting fraction of anhydrous milk fat acts as mobilizer/solvent of the high-melting fractions but also crystallizes itself [36]. The findings support previous work by van Aken [37]. Vereecken et al. [11] studied the effect of the molecular makeup (stearic versus palmitic acid-based) in fat blends of monoacid saturated TAGs and mono-unsaturated TAGs. According to their study, palmitic acid-based blends form mixed crystals, which generate better seeding effects than stearic-acid-based counterparts with the high-melting TAGs being the crystallization drivers.

From spread's and shortening's production it is known that the mixing behavior of the TAGs in the hardstock/fat blends plays a crucial role in preventing the migration of TAGs during storage and recrystallization into more stable polymorphic forms. This can yield in emulsion breakdown and is further associated with granular crystal formation and associated network properties [38–40]. Besides the addition of emulsifiers, fat blend formulation plays an important role. Fat modification including enzymatic interesterification has been proven useful in this field as method to control the amount of POP and POO—both important drivers for

granular crystal formation [38, 41, 42]. To the best of our knowledge, there is limited knowledge on the interplay of polymorphic transitions and mixed crystal formation and its effect on phase segregation.

In this contribution, four cases are discussed in which the recrystallization of the high-melting fraction in multicomponent palm oil-based fat blends was studied via DSC. In some cases, additionally time- and temperature-resolved SAXS/WAXS measurements were performed. Different techniques such as stabilization and annealing were applied to manipulate the crystallization. This collection of case studies aims to highlight the importance of careful data collection and interpretation of complex fat blends using DSC and provides examples of how annealing can be applied to manipulate mixed crystal formation in systems prone to phase segregation.

Material & methods

Material

Fully hydrogenated rapeseed oil (FHRO) was kindly provided by ADM (Hamburg, Germany). Refined, bleached and deodorized palm oil (PO) and a PO-based commercial hardstock (PCM) were provided by Flora Food Group B.V. (Wageningen, The Netherlands). According to the supplier, PCM contains 20.3% (m/m) fully saturated long-chain TAGs (H3), 23.6% (m/m) fully saturated TAGs with two long-chain and one medium-chain fatty acid (H2M), and 13.6% (m/m) mono-unsaturated TAGs (H2U; two long-chain saturated fatty acids and one unsaturated fatty acid). Multiple fractionated palm stearin (POSt) with an iodine value of 12 was kindly provided by AAK (Aarhus, Denmark). Refined rapeseed oil (RP) was contributed by Gustav Heess GmbH (Leonberg, Germany). Tripalmitin (PPP) with a purity of > 98% was purchased from ThermoScientific (Dreieich, Germany). All materials were used without further modification. The fatty acid composition of the blends analyzed is given in Table 1.

Methods

Calorimetry

All studies were performed via differential scanning calorimetry (DSC) using a 214 Polyma calorimeter (Netzsch, Selb, Germany). Approximately 8–13 mg of sample were weighed in aluminum crucibles and sealed hermetically. An empty crucible was used as reference. The temperature-time protocols varied in each case study and are described in the following.

Case study I The study was performed on PO (PO) enriched with 2% (m/m) FHRO (SSS-rich) and 3% (m/m) POSt (PPP-rich). This way, the total amount of H3 TAGs in both samples was 9.6 % but the distribution of stearic and palmitic acid in the H3 TAG melting group differed. To be precise, the POSt in PO sample was assumed to mainly contain tripalmitin (PPP) as H3 TAG, whereas the FHRO in PO mixture contained also tristearin (SSS) from the added FHRO, but mainly PPP from PO itself. Their ratio was 21/79 (SSS/PPP), which is close to the eutectic mixture of SSS/PPP [6, 43, 44].

To study the isothermal crystallization over time using DSC, the stop-and-return method by Foubert et al. [13] was adapted. In this, the sample is crystallized and re-melted after increasing isothermal holding times. In each cycle, the sample was subject to the same holding period of at least 10 min at 80 °C to eliminate any crystal memory, and a cooling rate of 10 °C min^{-1} ensured a similar supersaturation throughout all experiments. The isothermal holding times

Table 1. Fatty acid composition. Values are given in mass percentages % (m/m)

Fatty acid	FHRO[a]-PO	POSt[b]-PO	PO	PCM-1	PCM-2	PCM-3	PCM-4	PMC
C8:0	n.d.	n.d.	n.d.	1.4	1.3	1.2	1.1	1.5
C10:0	n.d.	n.d.	n.d.	1.2	1.1	1.0	0.9	1.3
C12:0	n.d.	n.d.	n.d.	16.5	16.0	14.5	13.1	18.3
C14:0	1.1	1.1	1.1	5.8	5.6	5.1	4.6	6.4
C16:0	44.2	45.7	45.0	49.3	50.4	54.3	57.7	54.3
C16:1	0.2	0.2	0.2	n.d.	n.d.	n.d.	n.d.	n.d.
C18:0	6.0	4.3	4.3	3.1	3.1	2.8	2.5	3.3
C18:1	37.2	37.4	37.9	17.5	17.2	16.1	15.2	12.3
C18:2	10.0	10.0	10.2	3.8	3.7	3.5	3.4	2.1
C18:3	0.2	0.2	0.2	n.d.	n.d.	n.d.	n.d.	n.d.
C20:0	0.4	0.4	0.4	0.2	0.2	0.2	0.2	0.2
Rest	0.7	0.7	0.7	1.3	1.3	1.3	1.3	0.3

[a]2% (m/m); [b]3% (m/m)

were 1, 2, 4, 6, 8, 10, 15, 30 min. The samples were held at 25 °C and the subsequent melting curves were evaluated. Those were obtained at different scan rates of 2, 5, and 10 °C min^{-1}. Peak temperatures were analyzed using the manufacturer's software. All measurements were performed in duplicate.

Case study II This study was performed on PO. DSC measurements were applied to follow the crystallization and melting events. First, the sample was held at 80 °C for 10 min to erase crystal memory. Then, the sample was cooled to -5 °C at 10 °C min^{-1} and held isothermally for 5 or 30 min. The melting was recorded at 2 and 10 °C min^{-1}. In a second scan, the sample was first crystallized at -5 °C as described above, then, the sample was partially melted at 5 °C for 5 min. The subsequent melting starting from 5 to 80 °C was recorded at 2 and 10 °C min^{-1}. The second temperature-time-profile was chosen to allow the sample to re-melt slightly at 5 °C, which introduced more mobility while keeping the supersaturation for initial crystallization high. All experiments were performed in duplicate.

Case study III This study was performed on a PO-based commercial hardstock (PCM) to which PPP (> 98% purity) was added. Blends were formulated such that the hardstock consisting of structuring TAGs (of the groups H3, H2M, and H2U) made up 90% of the blend and rapeseed oil as 'solvent' made up 10 %. The hardstocks were unmodified PCM and mixtures of PCM and PPP. This way, blends were created containing (1) 18.1% (m/m), (2) 19.9% (m/m), (3) 26.8% (m/m), and (4) 32.8% (m/m) TAGs of the H3 group in total. In the following, the blends are denoted as PCM-1, PCM-2, PCM-3, and PCM-4, according to the concentration in H3 TAGs as described above.

The samples were heated to 80 °C and held at that temperature for 10 min to remove any crystal memory. Subsequently, the samples were cooled at 10 °C min^{-1} to 10 °C. After holding the temperature for 30 min, the sample was heated to 80 °C at 2 °C min^{-1}. Peak temperatures and areas were analyzed using the manufacturer's software. All measurements were performed in duplicate.

Additionally, the samples were subjected to annealing during melting at 43, 45, and 48 °C for 45 min. The areas under the DSC curves obtained during melting were analyzed using the manufacturer's software. To avoid superposition of the short equilibration phase of the DSC instrument when beginning another heating phase (i.e., start-up hook), the melting did not start from 43, 45, 48 °C but 2 °C below. The rapid cooling by 2 °C was reached by a cooling rate of 40 °C min^{-1}. This procedure is assumed not to change the crystallized material substantially given to rapid cooling process. All measurements were performed in duplicate.

Case study IV The unmodified and undiluted PCM was subject to different temperature-time-profiles (Figure 1). In any profile, the sample was first heated to 80 °C and held at that temperature for 10 min to remove any crystal memory.

1a) The sample was cooled at 10 °C min^{-1} to 10 °C. After holding the sample for 30 min, the sample was heated to 80 °C at 2 °C min^{-1}.

1b) The sample was cooled at 10 °C min^{-1} to 10 °C. After holding the sample for 30 min, the sample was heated to 46 °C at 2 °C min^{-1}, held at that temperature for 10 min, respectively, and afterward further heated 80 °C at 2 °C min^{-1}.

1c) The procedure is similar to 1b) but during heating, the sample was annealing at 46 °C for 60 min before heating further to 80 °C.

2a) The sample was cooled at 10 °C min^{-1} to 35 °C, held at that temperature (annealing) for 60 min, and afterward further cooled at 10 °C min^{-1} to 10 °C. After holding the sample for 30 min, the sample was heated to 80 °C at 2 °C min^{-1}.

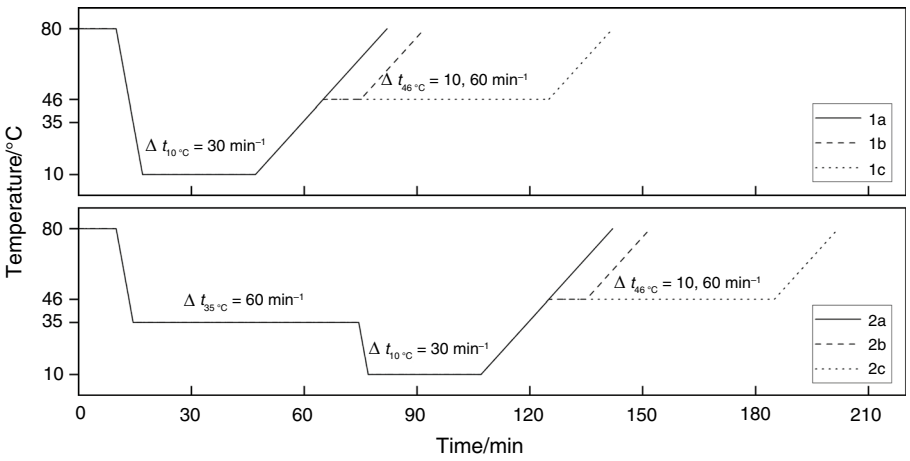

Fig 1 Temperature-time profiles applied in the annealing study

2b) The sample was cooled at 10 °C min^{-1} to 35 °C, annealed for 60 min, then further cooled at 10 °C^{-1} to 10 °C. The temperature was held for 30 min, after which the sample was heated to 46 °C at 2 °C min^{-1}, annealed for 10 min, respectively, and further heated at 2 °C min^{-1} to 80 °C.

2c) The procedure is similar to 2b) but during heating, the sample was annealing at 46 °C for 60 min before heating further to 80 °C.

X-ray Scattering measurements and analysis

Small-angle X-ray scattering (SAXS) and wide-angle X-ray scattering (WAXS) experiments were performed on the samples in cases I and IV, following the same temperature-time profiles as described above. All measurements were performed on a SAXSpace instrument (Anton Paar GmbH, Graz, Austria) using a Cu anode ($\lambda = 0.154$ nm) and operating at 40 kV and 50 mA. A TCstage 150 Peltier element (Anton Paar GmbH, Graz, Austria) allowed temperature control of the sample in the sample chamber. SAXS/WAXS measurements were performed simultaneously at a sample-detector distance of 130 mm. This covers a q range from 0.1 to 17.6 nm^{-1} ($q = 4\pi \sin(\theta)/\lambda$, with 2θ being the scattering angle). The 1D scattering patterns were recorded with a Mythen microstrip X-ray detector (Dectris Ltd., Baden, Switzerland). Quartz disposable capillaries (Capillary Tube Supplies Ltd., Cornwall, U.K.) with an outside diameter of 1.5 mm were used. The samples were melted on a hot plate before injection into the capillaries, which were sealed with wax afterward.

The X-ray patterns were collected during cooling, the isothermal hold and during melting. No continuous data collection during cooling and melting was possible. Therefore, X-ray patterns were collected in a step-wise fashion. SAXSTreat software (Anton Paar GmbH, Graz, Austria) and SAXSQuant software (Anton Paar GmbH, Graz, Austria) were used to setting the primary beam position to zero and normalizing for the sample transmission. Afterward, the pattern of an empty capillary was subtracted from each sample pattern. Further, the liquid contribution was subtracted for displaying of the diffraction content of the pattern. For further details, readers are referred to Seilert et al. [35].

Results and discussion

Case study I: isothermal crystallization of saturated monoacid TAGs in PO

Case study I presents the isothermal crystallization of PO enriched with saturated monoacid TAGs of different origin (FHRO is SSS-rich *vs.* POSt being PPP-rich). We note, that the POSt-PO sample is similar to PO with TAGs primarily dominated by palmitic and oleic acids. Further, POSt-PO meets the content of trisaturated TAGs of FHRO-PO. The crystallization was performed in a step-wise manner by increasing the isothermal holding time each cycle and evaluating the subsequent melting. Further, the heating rate was varied. This allows monitoring potential mixed crystal formation and polymorphic transition via DSC experiments. Figure 2A shows the melting curves of FHRO in PO and POSt in PO obtained with a scan rate of 2 °C min^{-1} after isothermal holding time of 1, 2, 4, 6, 8, 10, 15, and 30 min, respectively.

In Figure 2A, a low-melting peak at 29.9 °C becomes apparent, after which a recrystallization peak follows shortly. Later, a second melting peak at 40.5 °C occurs along with a doublet peak for the FHRO in PO sample. These two overlapping high-melting peaks appear at 43.9 and 45.4 °C, respectively. A comparable behavior can be observed for the reference system POSt in PO (Figure 2B). However, the overall crystallization is less complex, e.g., only one high-melting peak is visible at 49.2 °C.

The identified endothermic and exothermic events in Figure 2A can be plotted over the isothermal holding time preceding the melting; see Figure 3A. Since a low heating rate was applied for the data acquisition, the time at which an event was detected was also dependent on the heating rate. The total time before an event was recorded (either endothermic or exothermic) is defined as the time given by the time of isothermal hold plus the time it takes to record a specific event. We, note the latter is a function of the scan rate. For instance, the second melting event after an isothermal hold of one minute occurs at 40.5 °C, which refers at a scan rate of 2 °C min^{-1} to an additional time of 7 min and 45 sec. A correction of the isothermal holding time for the applied heating rate of 2 °C min^{-1} is depicted in Figure 3B.

Considering the total elapsed time for calorimetric detection of events (Figure 3B), the high-melting peaks (the second melting event, the shoulder, and the doublet peaks) are expectedly registered at a later time. In contrast, in the first few minutes one fraction of the blends crystallizes that quickly recrystallizes again. Hence, the high-melting peaks observed after short isothermal holding times appear relatively later due to the low scan rate. Here, the sample undergoes a transition during the heating process. This also implies that initially only material crystallizes that becomes supersaturated at higher temperatures during the melting, i.e., concerning the high-melting TAGs in SSS- and PPP-rich mixed crystals.

Further, it is worth noting that some events appear at lower temperatures with increasing isothermal holding times. This is surprising as it is counterintuitive; commonly an increase in melting point temperature is expected with an increase in the amount of crystallizing material. A polymorphic form of higher stability also shows a higher melting

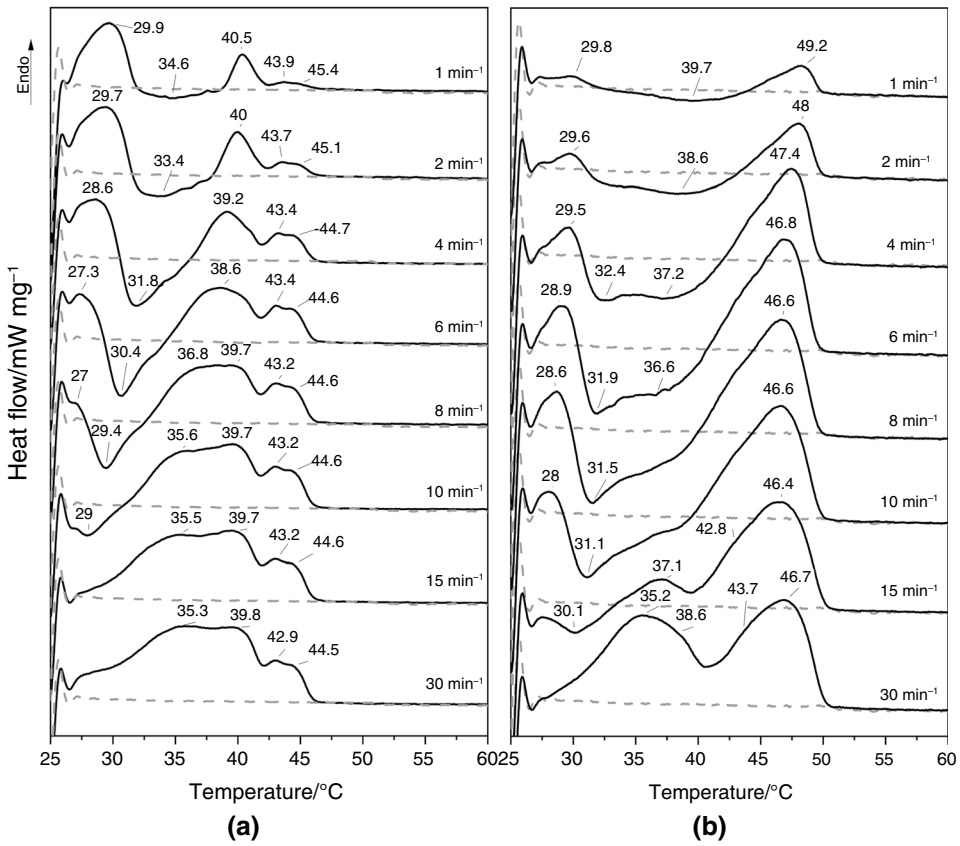

Fig 2 DSC melting curves of **A** FHRO in PO and **B** POSt in P after crystallizing at 25 °C for different isothermal times obtained at 2 °C min^{-1}. Identified endothermic and exothermic peaks as indicated. All temperatures in °C. Rapeseed oil without any crystallizing material added is given as dashed lines for reference

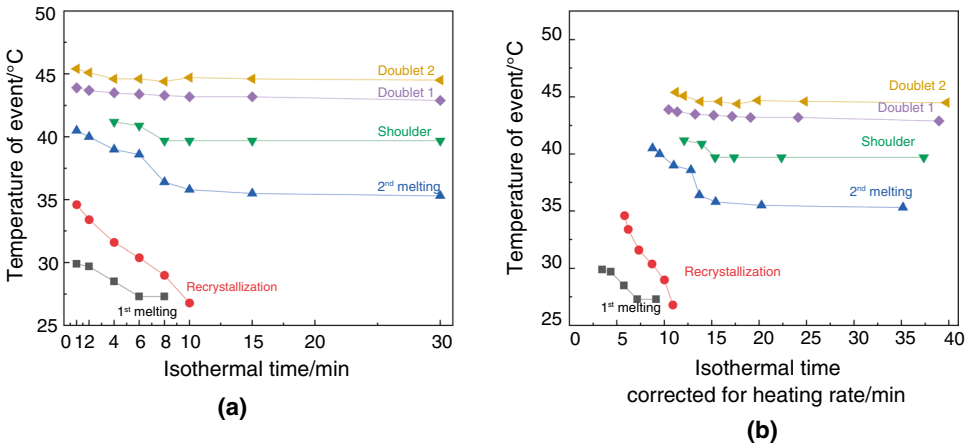

Fig 3 **A** Temperature of event plotted against the isothermal time and **B** temperature of event plotted against the isothermal time corrected for the applied heating rate for FHRO-PO blend. The transition temperatures relate to Figure 2A

temperature taken the composition remains unchanged. This indicates, that the composition of the mixed crystal phases changes with the isothermal holding time. This renders the crystallization process particularly time-dependent, affecting not only the amount of crystallized material (increase in melting temperature) but also its composition. Here, the decrease in event temperatures allows two interpretations: (1) the longer the isothermal phase, the more lower-melting TAGs are incorporated into the mixed crystal phases, ultimately lowering the melting temperature; and (2) the polymorphic transition proceeds with increasing isothermal holding time reducing the amount of the α-phase (1st melting peak) and, hence, less material dissolves/recrystallizes, resulting in lower temperatures.

After a certain time, no first melting peak and no recrystallization is observed during the melting, and the melting events do not change in temperature.

The step-wise crystallization routine and the evaluation of the subsequent melting can be performed for different heating rates (also 5 and 10 °C min^{-1}) (Figure 4). The

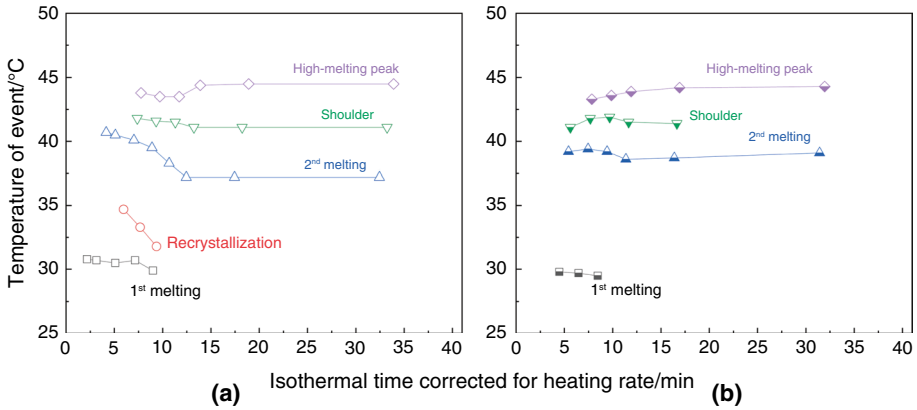

Fig 4 Temperature of event plotted against the isothermal time corrected for the applied heating rates **A** 5 and **B** 10 °C min^{-1} for FHRO-PO

respective DSC curves are given in the Supporting Information (Figure S1).

It becomes apparent that at higher heating rates less thermal events are recorded. For example, the doublet peak observed at the low scan rate of 2 °C min^{-1} becomes a single high-melting peak at higher scan rates. This is due to increasing peak intensities and peak broadening resulting from the superposition or overlapping of different events. For every heating rate, the first melting peak is still present when the second melting peak and the higher melting peak emerge. The high-melting peaks (approx. 44 °C) identified earlier as recrystallized from released and then supersaturated high-melting material are still detectable as shoulders of the main melting events, when applying higher scan rates. Further, for every heating rate, the second melting peak decreases with longer isothermal holding times. Applying a low heating rate (2 °C min^{-1}) allows detecting the two overlapping high-melting peaks, which are otherwise not resolved due to the peak broadening when applying higher heating rates. However, the slow heating also allows the sample to restructure during the melting. While this introduces an artifact, it also allows to gain insights into the crystalline state at the beginning of the melting, i.e., degree of incorporation of high-melting TAGs. Here, a double high-melting peak observed for FHRO in PO indicates the separate melting of two H3-rich phases, one rich in SSS, the other rich in PPP. In contrast, only one high-melting peak was observed for the P-based counterpart blend POSt in PO (Figure 2B).

The time correction for the calorimetric detection of events described above was also performed on POSt-PO (Figure 4). The respective DSC curves are given in the Supporting Information (Figure S2).

In comparison with FHRO-PO, POSt-PO shows a more simple crystallization and melting behavior.

To verify the polymorphic forms and to understand the crystal packing (lamellar staking), SAXS/WAXS analyses were performed following the same temperature-time profile, i.e., allowing the sample to crystallize for different times (6, 10, 15 min, and 30 min), and evaluating the subsequent melting (Figure 5). In line with the DSC experiments, a cooling rate of 10 °C min^{-1} and a heating rate of 2 °C min^{-1} was applied. The experiments were performed on both samples (FHRO and POSt in PO). The d-spacings obtained from SAXS and identified polymorphic forms from WAXS during melting are shown in Figure 6.

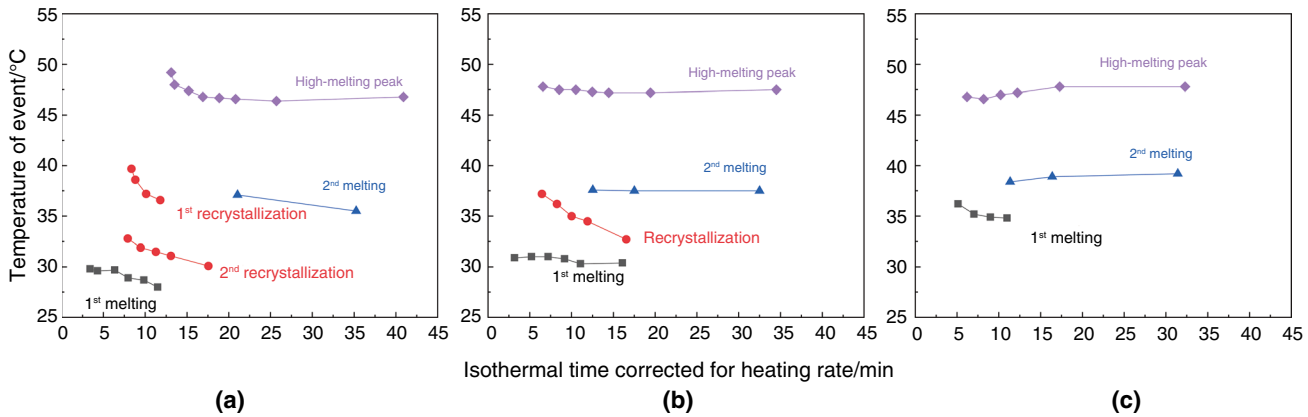

Fig 5 Temperature of event plotted against the isothermal time corrected for the applied heating rates **A** 2, **B** 5, and **C** 10 °C min^{-1} for POSt-PO

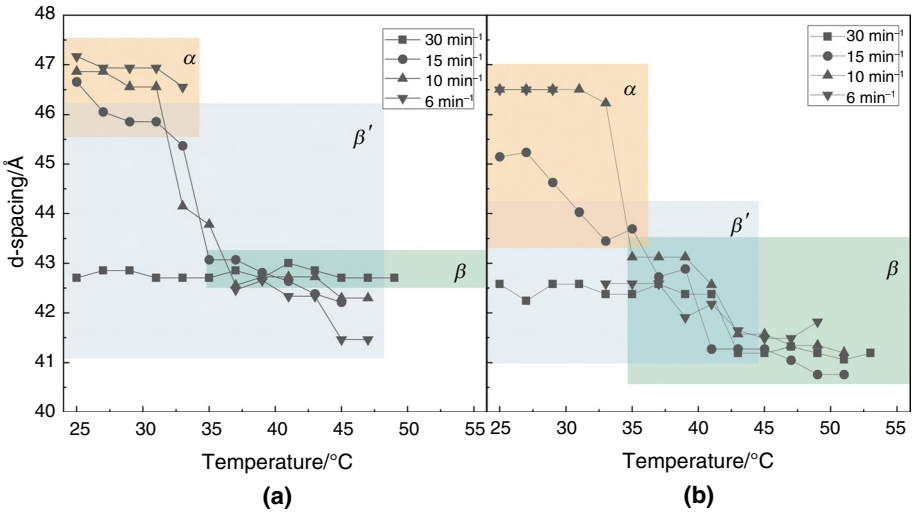

Fig 6 Evolution of d-spacing in SAXS region recorded during melting at 2 °C min^{-1} for **A** FHRO in PO and **B** POSt in PO after increasing isothermal holding times: 6 min (downward facing triangles), 10 min (upward facing triangles), 15 min (circles), 30 min (squares). Polymorphs are identified from WAXS pattern and color-coded as: α (orange), β' (blue), β (green). Overlapping regions indicate co-existing crystalline phases assigned to the same d-spacing. Figure taken with permission from ref. [35]

When crystallizing FHRO in PO only for 6 min, the initial d-spacing at the start of the melting is 47 Å. This can be assigned to an α phase. The d-spacing decreases when the sample is given more time to crystallize, 10 and 15 min, resulting in a d-spacing of 46.5 Å and 46 Å, respectively. This indicates either a different packing and/or composition. After 30 min of crystallization time, the d-spacing is 43 Å relating to only a β' polymorph. This is in line with the peak temperatures and their shifts over increasing isothermal holding time in DSC.

The POSt in PO sample shows an initial d-spacing of 46.5 Å also relating to an α-polymorph. This d-spacing decreases only after 15 min with a drop more drastically observed than for FHRO in PO. Also, the POSt in PO sample shows a dominating β phase in the end, which can be traced by the three-step evolution of the d-spacing during melting. The initial d-spacings of FHRO in PO are slightly larger than those of POSt in PO. This indicates the disturbance a small amount of SSS causes in PPP-dominated crystal structures.

Comparing the information obtained from SAXS and WAXS data to the DSC signals obtained after various holding times, it becomes apparent that both techniques complement each other. The DSC signal offers the melting characteristics, endothermic and exothermic events while the SAXS/WAXS measurements give insights into the polymorphic state and the lamellar spacings at a given temperature and time. The observed d-spacing and polymorph information of FHRO in PO reveal that the first melting corresponds to an α phase and the second melting and doublet peak most likely correspond to two separate β phases. Further, the temperatures of the respective events decrease with increasing isothermal holding times (Figure 2A), which coincides with the decrease in d-spacing. Similarly, the initial (start of the melting) and final d-spacings (end of melting) change with the isothermal holding time applied (Figure 6A). For POSt in PO, the d-spacing at the beginning of the melting only changes after 15 min isothermal time (Figure 6B). This corresponds well to the DSC signal (Figure 2B). The first melting is almost not visible whereas the second melting starts to become more pronounced followed by the high-melting that is fully developed.

The results illustrate the difficulty that lies in the interpretation of DSC curves for multicomponent systems. This holds especially for systems for which a tendency to polymorphic crystallization and fractionation, i.e., selective co-crystallization, is well-documented as in the case for PO [10, 18, 21, 32, 33] and, recently, for the blends at hand by our group [35]. Further, taking into account the vast amount of TAGs in modern commercial blends (but also in PO), assigning only one polymorphic transition of an invariable phase composition to any multiple-step crystallization process seems in the light of our studies rather unjust. The TAGs likelihood to form mixed crystalline phases of different composition must be considered. This evidently complicates the matter at hand even further. Ultimately, when SAXS/WAXS analyses are not readily available, step-wise crystallization experiments using DSC offer an appropriate alternative, when multiple scan rates are explored.

Case study II: modulation of PO's fractional crystallization by variation of time temperature profiles

In this study, PO was subject to different temperature-time-profiles. The aim was to manipulate the crystallization in such a way that the recrystallization of high-melting TAGs, namely PPP, during the heating scan gets suppressed. PO was subject to fast cooling (10 °C min^{-1}) to − 5 °C and to 5 °C for 5 and 30 min. In another run, the sample was allowed to partially melt at 5 °C for 5 min after the first isothermal step at − 5 °C. This allowed the sample to re-melt slightly introducing more mobility while

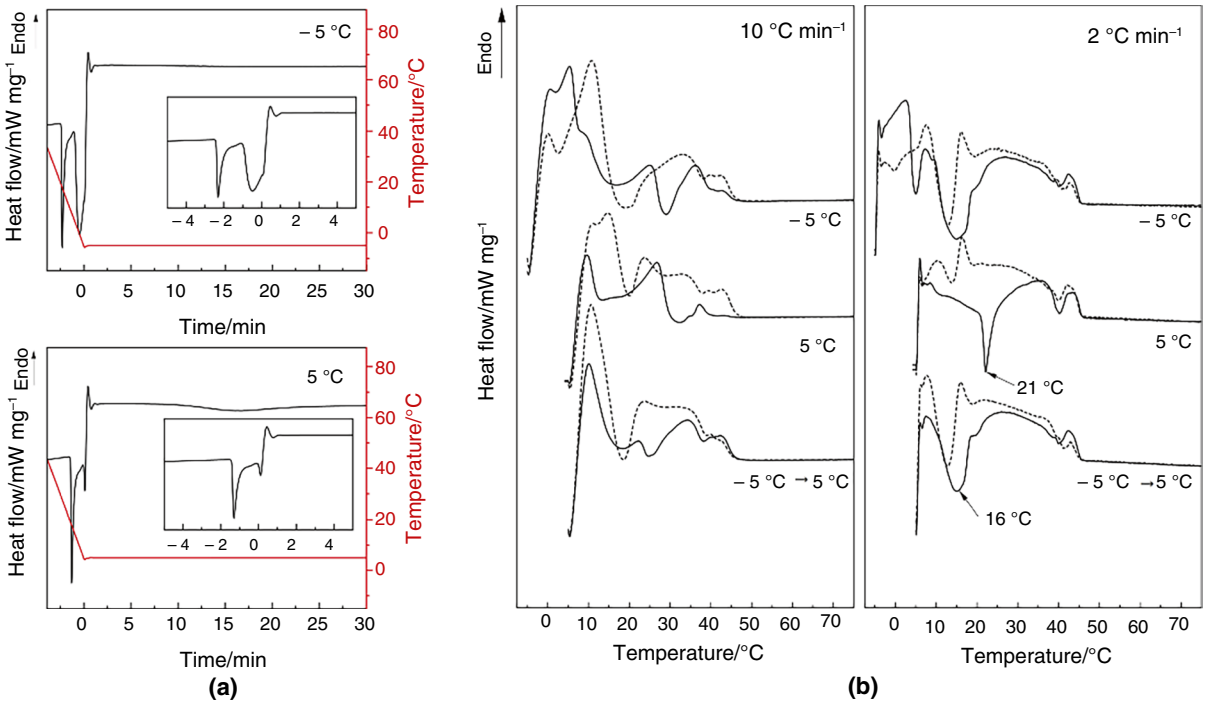

Fig 7 **A** Time-resolved DSC signal of the isothermal crystallization for 30 min at −5 (solid line) and 5 °C (dashed line). The start of the isothermal phase was set to zero. **B** Melting curves obtained of PO when crystallized at −5 or 5 °C for 5 min (solid line) and 30 min (dashed line) and when subjected to annealing at 5 °C for 5 min; crystallization temperatures as indicated. Left: melting curves obtained with a scan rate of 10 °C min^{-1} and right: 2 °C min^{-1}

keeping the supersaturation for initial crystallization high. Figure 7A gives the time-resolved DSC signal of the crystallization at −5 and 5 °C. Melting curves were obtained at 2 and 10 °C min^{-1} and are shown in Figure 7B.

When crystallized at 5 °C, the first exothermic event was recorded during the cooling phase, the second after 15 min in the isothermal period (Figure 7A). When crystallized at −5 °C, both crystallization events are recorded during the cooling—see negative times. This is also reflected in the melting curves revealing a smaller high-melting peak at approx. 40 °C when crystallized only for 5 min (Figure 7B). The effect of crystallization time is diminished when a lower heating rate of 2 °C min^{-1} is applied. This is because the additional time allows the sample to recrystallize during the slow temperature increase.

In incomplete crystallization at 5 °C for only 5 min is also evident from the sharp exothermic event recorded at 21 °C during the melting at 2 °C min^{-1} (Figure 7B). Here, applying a longer isothermal holding time (30 min) or slow heating rate (2 °C min^{-1}) both result in considerable high-melting peaks but of different magnitudes. Interestingly, both events, the second crystallization at 5 °C and the recrystallization at 21 °C result in similar high-melting peaks applying a scan rate of 2 °C min^{-1}. The indifference to temperature implies that only PPP and related high-melting TAGs recrystallize.

When heating at 2 °C min^{-1}, all crystallization regimes (−5 °C or 5 °C) show a comparable high-melting peak when crystallized for only 5 min. When the crystallization time was increased to 30 min, the high-melting peak differs with the crystallization temperature. The peak is greater when PO is crystallized at 5 °C as compared to −5 °C. Considering only the melting DSC curve obtained when crystallized at 5 °C, the high-melting peak area increases with the time (5 min < 30 min). Interestingly, this is not the case when PO was crystallized at −5 °C. This is counterintuitive, as more time usually results in more material crystallizing. While this certainly is the case in a general sense considering the area under the DSC curves (solid *versus* dashed lines in Figure 7A), the effect of crystallization time on the high-melting peak resulting from a melt-induced recrystallization has to be discussed in more detail. In this study, the data suggest that the crystallization of PPP (the high-melting component in PO) and its incorporation into a mixed crystal phase is a time-dependent process. The more time PO is given to crystallize more material, e.g., mono-unsaturated TAGs, crystallizes. In the process, the solid phase undergoes a change in composition, which results in less PPP being released during melting which is able to recrystallize from the supersaturated liquid.

Lastly, PO was crystallized at −5 °C for either 5 or 30 min and afterward subjected to a partial melting step at

5 °C for 5 min only. The melting curves are also given in Figure 7B. Here, the shorter crystallization time of 5 min results in a greater high-melting peak regardless of the scan rate applied. This suggests that when allowing the sample to crystallize for longer a better crystal packing is supported. This results in less PPP being released. The difference in the high-melting peak is diminished when heating at 2 °C min^{-1}. However, here, an exothermic event at 16 °C was recorded when the sample was given only 5 min in the first isothermal phase (Figure 7B).

The results allow the following interpretation: if initially an appropriate supersaturation is given, a PPP-rich α-phase is formed (first crystallization event in Figure 7A), after which other mixed crystals of varying composition are formed (second crystallization event). The α-phase can recrystallize during the isothermal hold (30 min at 5°C) or during the melting at 2 °C min^{-1}. The recrystallization of a PPP-rich phase is further aided by partial melting/annealing at 5 °C for 5 min. The partial melting of low-melting material increases the mobility in PO allowing solid-solid transition during the isothermal holding period at 5 °C and recrystallization later during the heating scan. This is in line with previous work on milk fat, in which the low-melting fractions acted as mobilizer or solvents for the high-melting fractions [36, 37]. The same could be observed, when PO was only crystallized at 5 °C. Here, the recrystallization is not to be confused with a melt-mediated polymorphic transition of a phase not changing in composition.

Overall, a greater mobility allows PPP-rich phases to recrystallize into a more stable polymorphic form, and thus, initiate phase segregation. This was observed for different temperature-time-conditions: (1) when the sample was given less time to crystallize, (2) the crystallization temperature was too high decreasing the overall supersaturation, (3) a low heating rate was applied, allowing the sample to restructure further aided by melting of low-melting material during the scan, and, (4), by partial melting at an elevated temperature.

In conclusion, gathering data on mixed crystal formation and melting properties via DSC is a matter of process parameters, including temperature, supersaturation, heating rates *versus* annealing procedures and careful data interpretation. In this study, applying a low heating rate, crystallizing for longer, and allowing the sample to partially melt did result in similar melting curves of PO.

Case study III: PPP-driven phase segregation in PCM

In this study, a palm-oil-based commercial hardstock (PCM) was spiked with PPP to investigate the phase separation driven by PPP. The aim was to facilitate the recrystallization of high-melting TAGs, namely PPP, resulting in a phase separation. The blends PCM-1, PCM-2, PCM-3, and PCM-4 comprise 18.1, 19.9, 26.8, and 32.8 % (m/m) of H3 TAGs, respectively, with the H3 fraction mostly containing PPP.

Figure 8 shows the DSC curves obtained for the four blends after cooling at 10 °C min^{-1} to 10 °C, 30 min isothermal crystallization, and subsequent melting at 2 °C min^{-1}.

The melting curve of PCM without additional PPP (18.1 % H3 in the blend, denoted as PCM-1) shows a minor recrystallization event at 45.4 °C and a subsequent melting peak at 49.1 °C. This high-melting peak increases for the samples PCM-2, PCM-3, and PCM-4 with increasing amounts of added PPP. Further, the recrystallization temperature decreases from 45.4 °C (PCM-1) to 42.4 °C (PCM-4). The blends with the greatest amount of added PPP, PCM-3 and PCM-4, both exhibit a shoulder of the high-melting peak at 47.6 and 46.5 °C, respectively. A similar overlap of melting peaks can be also assumed for the samples PCM-1 and PCM-2, however, the DSC data of the melting scan do not allow to resolve the events.

The area of the high-melting peak and its share of the total area were determined and plotted against the known H3 concentration in the blends (Figure 9).

The area of the high-melting peak increases with the concentration of the PPP-dominated H3 fraction. Here, the high-melting peak reflects the recrystallization of PPP from a supersaturated melt. To determine whether PPP assumes the β' or β polymorph, its solubility can be calculated.

The Hildebrandt equation describes the ideal solubility of a component *i*, assuming an ideal liquid phase, negligible changes in the heat capacity, and a pure solid phase. The ideal solubility of PPP can be calculated as follows: Eq. (1)

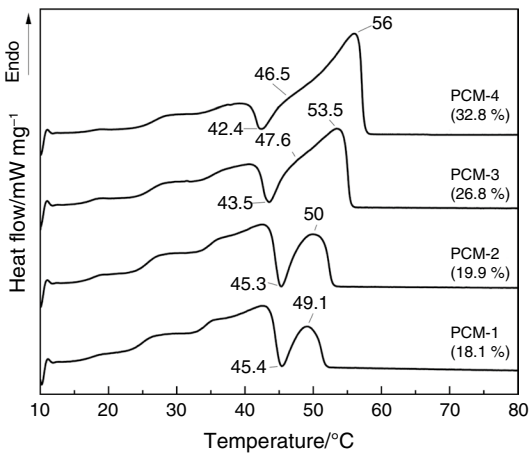

Fig 8 Melting curve of PCM mixed with PPP obtained at 2 °C min^{-1}. PCM-1 denotes the hardstock and PCM-2, PCM-3, PCM-4 denote samples with increasing amounts of added PPP. Identified endothermic and exothermic peaks as indicated. All temperatures in °C

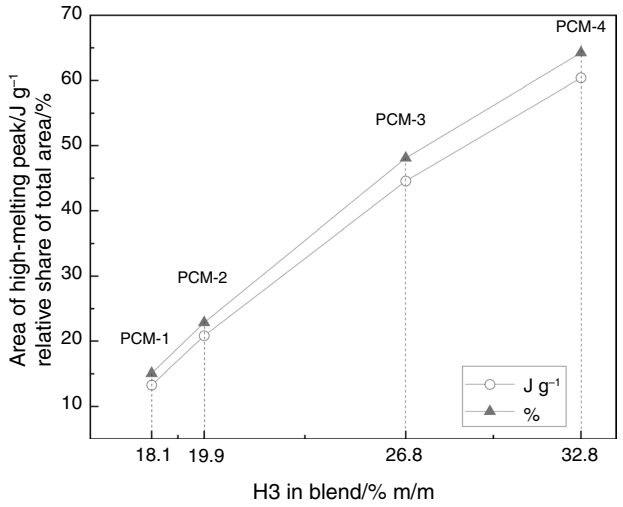

Fig 9 Area of high-melting peak (empty circles) and its relative share of total area (filled triangles) under the DSC curve plotted against the total H3 concentration in the blends

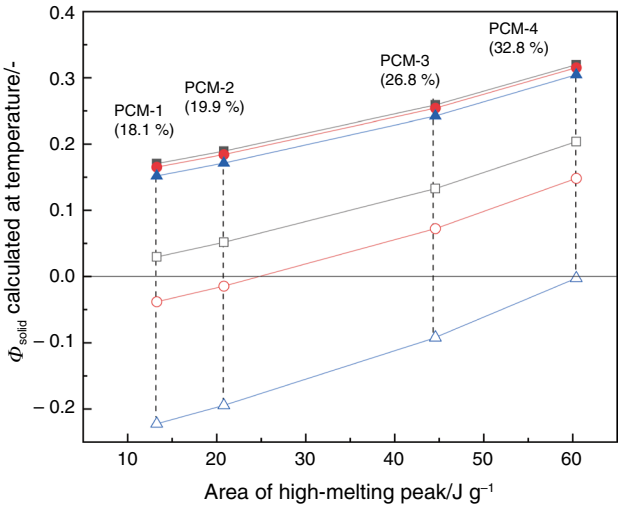

Fig 10 Calculated amounts of solids in β' (empty symbols) and β (filled symbols) for 43 °C (black), 45 °C (red), and 48 °C (blue) plotted against the area of the high-melting peak. Dashed lines to guide the eye

$$x_i^L = \exp\left(-\frac{\Delta h_i^{\text{fusion}}}{\text{R T}}\left(1-\frac{T}{T_i^{\text{sl}}}\right)\right) \quad (1)$$

where x_i^L denotes the molar fraction of PPP in the liquid phase, $\Delta h_i^{\text{fusion}}$ is the enthalpy of fusion of PPP in either α, β' or β, R is the ideal gas constant, T is any temperature, and T_i^{sl} denotes the melting point temperature of either the α, β' or β polymorph. For PPP, $T^{\text{sl}} = 55.7$ °C and $\Delta h^{\text{fus}} = 126.5$ kJ mol^{-1} and $T^{\text{sl}} = 65.9$ °C and $\Delta h^{\text{fus}} = 171.3$ kJ mol^{-1} were used for β' and β, respectively [6]. This way, the solubility of PPP in the liquid phase in either β' or β at any temperature, T, can be calculated. It must be noted, that here the liquid phase is postulated an ideal solution and the high-melting peak to consist of PPP exclusively. Considering the peak shape and the tendency of mixed crystal formation in systems containing H3 and H2M TAGs as documented by our group [45] leaves this assumption doubtful.

The amount of solids was calculated obeying mass balance as follows: Eq. (2)

$$\Phi_{\text{solid}} = \frac{x_{\text{PPP}}^{\text{mix}} - x_{\text{PPP}}^L}{1 - x_{\text{PPP}}^L} \quad (2)$$

Here, $x_{\text{PPP}}^{\text{mix}}$ denotes the known PPP concentration (simply the H3 concentration), x_{PPP}^L gives the amount of PPP in the liquid phase calculated via Eq. (1). Ultimately, Φ_{solid} gives the solid fraction at the temperature.

This further allows to predict the area under the high-melting peak ($\Delta h_{\text{predicted}}^{\text{dissolution ideal}}$) assuming ideal dissolution of PPP in either β' or β, Eq. (3)

$$\Delta h_{\text{predicted}}^{\text{dissolution ideal}} = \Phi_{\text{solid}} \cdot \Delta h_{\text{PPP}}^{\text{fusion}} \quad (3)$$

Figure 10 shows the amount of solids (Φ_{solid}) calculated for different temperatures, 43, 45, and 48 °C, for the β' and β-polymorph plotted against the measured area of the high-melting peak.

It becomes obvious that the β phase is the most viable. Small amounts of a β' phase can also be expected at 43 °C assuming ideal dissolution of a neat PPP phase. This temperature is below the recrystallization peak temperature observed for PCM-1 and PCM-2 (Figure 8). For the blends PCM-3 and PCM-4, the recrystallization temperatures of 43.5 and 42.4 °C are in good agreement with the amount of solids calculated for a β' phase at 43 and 45 °C. It must be noted, that the imperfect peak shape of the high-melting peak for both samples suggests impurities of the fraction melting. These impurities can be related to the polymorphic phases, β' and β, and to differences in their composition, i.e., not only PPP is melting but a PPP-rich mixed crystal.

The calculated amount of solids formed assuming ideal solubility were used to predict the enthalpy, i.e., area, of PPP at 43 °C, 45 °C, and 48 °C. Figure 11A shows the predicted area under the high-melting peak ($\Delta h_{\text{predicted}}^{\text{dissolutionideal}}$) calculated for the β' and β-polymorph plotted against the measured area of the high-melting peak.

Here, data points close to the ideal prediction indicate ideality in the equilibrium state. The predictions for the β-polymorph are closer to the experimental data except for PCM-1 and PCM-2. The overprediction observed for the β-polymorph can be assigned either to non-ideality or imperfect crystal packing.

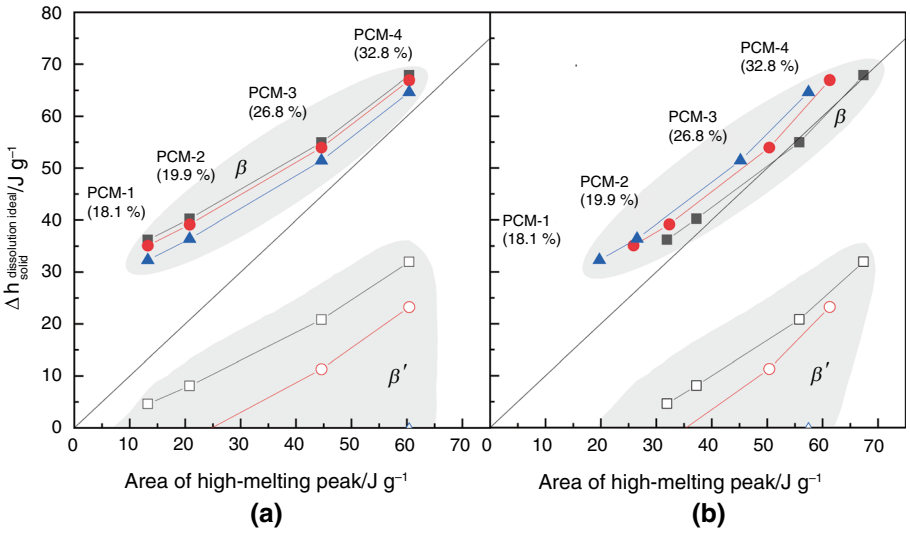

Fig 11 Predicted area for β' (empty symbols) and β (filled symbols) assuming ideal dissolution of PPP at 43 °C (black), 45 °C (red), and 48 °C (blue): **A** plotted against the measured area of the high-melting peak and **B** plotted against the measured area of the high-melting peak obtained after annealing at 43, 45, and 48 °C

The recrystallization of the PPP-dominated H3 fraction was promoted by annealing the samples during melting at different temperatures, being 43, 45, and 48 °C for 45 min. Figure 11B shows the parity plot of the predicted area under the high-melting peak plotted against the measured area. The DSC curves obtained after annealing for all samples are depicted in Figure S3 in the Supporting Information. The DSC curves obtained after annealing also show peak broadening. Again, this can be attributed to multiple melting events taking place not limited to the polymorphic transition. PCM is of PO-origin rendering the H3 fraction PPP-dominant but it also includes stearic-acid containing TAGs. Further, H3 and H2M TAGs can form mixed crystals (M: medium-chain fatty acids as lauric (La) and myristic (My) acid). Although the literature data on those are scarce, it has been reported that the chain length differences determine whether the TAGs are β' or β-tending, e.g., β is the most stable polymorphic form for PPC (1,2-dipalmitoyl-3-decanoyl-*sn*-glycerol) and PPLa (1,2-dipalmitoyl-3-lauroyl-*sn*-glycerol), whereas β' is the most stable form reported for PPMy (1,2-dipalmitoyl-3-myristoyl-*sn*-glycerol) [46, 47]. Similarly, its symmetrical counterpart PMyP (1,3-dipalmitoyl-2-myristoyl-*sn*-glycerol) and other symmetrical TAGs with chain length differences of +2 C-atoms at the *sn*2-position were reported to be β' tending [48]. As the general chain length differences between PPMy, PPLa, and PPP are relatively small, so are the differences in crystal packing as long spacings reported to be approx. 40 Å in the β-polymorph [49]. This generally supports the conclusion that those TAGs are likely to form mixed crystals due to their structural similarities. Interestingly, the binary system PPP/MyMyMy is also miscible in every polymorphic form [50]. This further underlines a deviation from ideality due to mixed crystal formation.

For the samples in this case study, applying annealing, specifically at 43 °C, results in a better agreement of experimental data to ideal calculations. Here, annealing allows a more perfect crystal packing of the PPP-rich phase recrystallizing/rearranging into a β phase.

In any case, the melting curves obtained for the PCM enriched with PPP and the annealing tests revealed a significant increase in phase segregation during the melting process directly related to the increasing amount of added PPP. High-melting TAGs as phase segregation drivers have been reported before [38, 39]. This further underlines that knowledge of a fat blends composition and thorough DSC analysis enables to understand the likeliness of segregation processes.

Case study IV: annealing to stabilize mixed crystal phases

Case study IV presents the crystallization and melting of a PO-based hardstock (PCM) subjected to annealing. The melting profiles are displayed in Figure 12.

In the standard profile (1a), the sample was crystallized at 10 °C min^{-1} to 10 °C, held there for 30 min, and afterward melted at a rate of 2 °C min^{-1}. During the melting, a recrystallization peak at 46.4 °C becomes visible after which a pronounced endothermic peak with a maximum at 50.2 °C was recorded. Subjecting the sample to annealing at 46 °C for 10 min or 60 min resulted in the melting curves 1b and 1c, respectively. The formerly sharp peak became broader, showing two peaks merged, and has overall a larger area.

Applying annealing during the cooling process is another variation. The melting curve obtained after annealing for 60 min during cooling at 35 °C (2a), which is approx. 10 °C below the recrystallization temperature of the same sample showed no recrystallization taking place and no additional

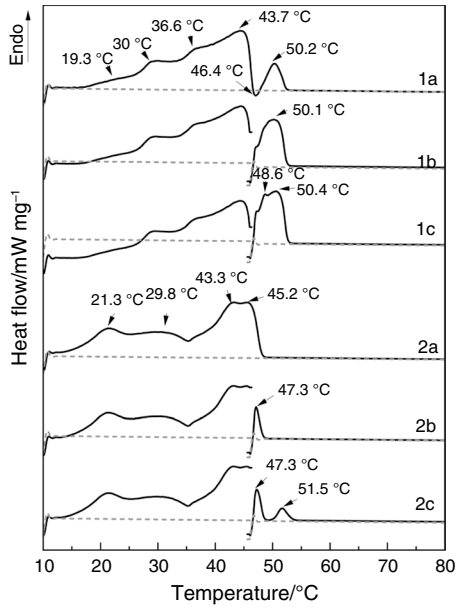

Fig 12 Melting curves obtained for PCM after applying different temperature-time-profiles: Cooling at 10 °C min^{-1} to 10 °C, isothermal holding time of 30 min before reheating at 2 °C min^{-1} (1a). Introducing annealing during cooling at 35 °C for 1 h results in the DSC curve (2a). Expanding 1a by applying annealing during heating for 10 or 60 min results in 1b and 1c, respectively. Expanding 2a by applying annealing during heating for 10 or 60 min results in 2b and 2c, respectively. Annealing at 46 °C introduced discontinuity in the melting DSC curves. The DSC signal obtained for rapeseed oil without any crystallizing material added is given as gray dashed lines for reference

endothermic peak at 50 °C compared to the standard profile (1a). Subjecting the sample following the crystallization route in 2a to annealing at 46 °C, 10 minutes (i.e., the presumed recrystallization temperature) resulted in the melting curve 2b showing a melting event at 47.3 °C. Extending the annealing during heating to 60 min resulted in two peaks at 47.3 and 51.5 °C (2c).

The data indicate that the annealing during the cooling process resulted in a different mixed crystal formation, which appears to hamper the release of PPP during melting and the subsequent recrystallization of PPP. This can be seen in the minor endothermic event at 47.3 °C. When the annealing is increased to 60 min, more released PPP recrystallizes from the liquid.

Using the Hildebrandt equation, the melting temperature of PPP in PCM can be calculated assuming the H3 fraction in PCM consists solely of PPP for the sake of simplicity. Accordingly, the dissolution temperature of 20.3% (m/m) PPP is 44.7 °C and 57.2 °C in the β' and β polymorph, respectively. The observed melting events are in between these temperatures.

The polymorphic crystalline state achieved at the end of the cooling process and its evolution during the heating were investigated via SAXS/WAXS measurements. Figure 13 gives the SAXS/WAXS pattern obtained following the temperature protocols 1a and 2a.

Without annealing during cooling (1a), the sample crystallized mostly in the α polymorph with a small amount of a co-existing β' phase also appearing. The 3rd order reflection (003) shows two separated peaks, observed at q = 4.14 nm^{-1} and q = 4.64 nm^{-1} related to α and β', respectively. This can be also observed in the 1st order reflection which exhibits a shoulder. After 30 min isothermal holding time, most of the α phase has transitioned into β'. In contrast, when the sample was subjected to annealing during the cooling phase (2a), no α phase was observed at the beginning of the isothermal holding time (Figure 13). The time-resolved DSC signals obtained during the cooling processes (1a and 2a) are given in the Supporting Information, Figure S4. Following the crystallization without applying annealing (1a), two crystallization events were recorded, at 25.7 °C and quickly afterward at the beginning of the isothermal holding time at 10 °C. Here, the first event corresponds to the formation of an α phase, the second to the formation of a β' phase. Since the α phase remains present for the isothermal holding time of 30 min, the signals cannot be attributed to a polymorphic transition of one phase but two separate phases present differing in polymorphic form and composition. When applying annealing in the cooling step at 35 °C (2a), a crystallization event is recorded during the annealing and later at 19.7 °C. Each event relates to a β' phase (Supporting Information, Figure S5) differing in supersaturation and, hence, in composition.

Overall, the β' phases observed at the end of the crystallization procedure in 1a and 2a differ in composition. This becomes clear comparing the d-spacings of 41.82 and 41.37 Å for the β' phase for 1a and 2a, respectively. Further, slightly different short spacings were observed in the WAXS region: 4.21 Å and 3.85 Å for 1a and 4.26 Å and 3.83 Å for 2a.

Furthermore, the SAXS/WAXS pattern were obtained during melting at a rate of 2 °C min^{-1} and annealing at 46 °C for 60 min—comparable to the DSC data discussed above—and are given in Figure 14. The SAXS/WAXS pattern obtained during the annealing at 46 °C in the heating step are given in the Supporting Information (Figures S6 and S7). It must be noted, that the temperature at which events occur cannot easily be compared due to the different thermal lag of the instruments.

Following the temperature profile 1a, the α and β' phases melt below 30 °C. Then, the sample transitions from the β' into the β polymorph. The β-polymorph is more pronounced after annealing for 60 min at 46 °C as seen for the temperature profile 1c. On the contrary, following the temperature profile 2a, the β' polymorph melts without any transition into β. The same can be observed in

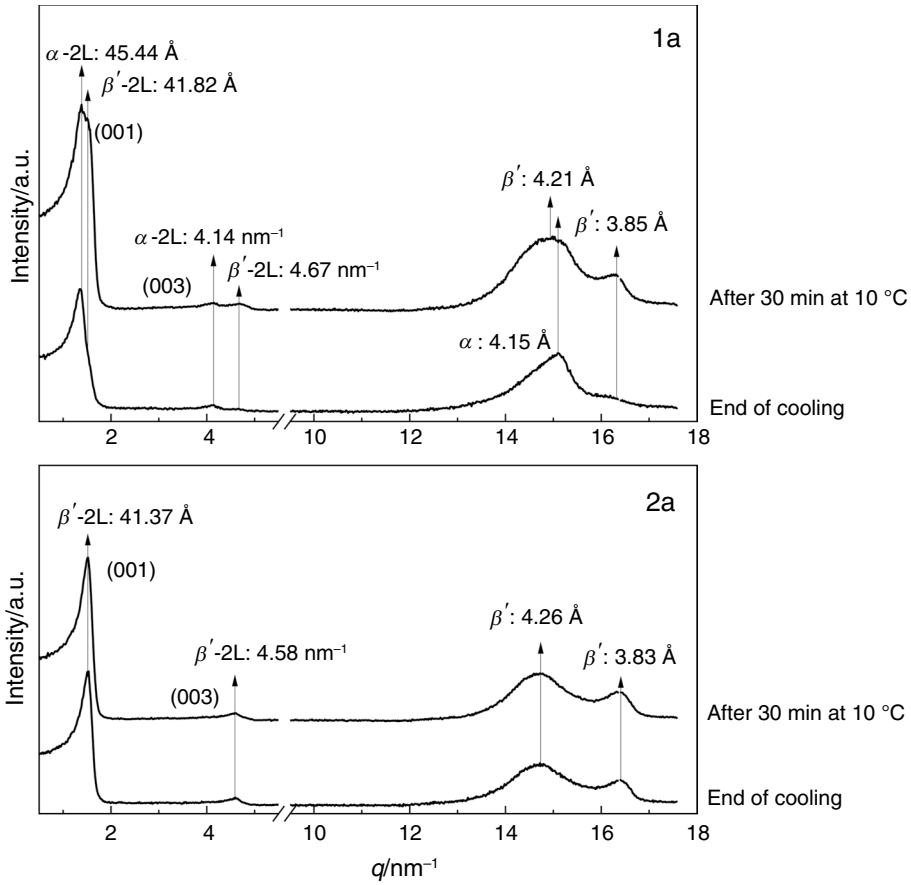

Fig 13 SAXS/WAXS pattern after subtraction of the molten signal (obtained at 70 °C) obtained at the end of the cooling phase and after 30 min isothermal hold at 10 °C for PCM subject to thermal protocol 1a (top) and 2a (bottom)

the SAXS/WAXS pattern obtained following temperature profile 2c. Here, no β phase was detected. The DSC curves showed two high-melting peaks at 47.3 and 51.5 °C (2c in Figure 12). Following the temperatures of the high-melting peaks observed for 1c one could be tempted to assume that the phases melting at 47.3 and 51.5 °C are a *β*' and a *β* phase, respectively. However, the WAXS pattern are opposing this notion as they only show a *β*' phase up until 52 °C and from 54 °C onwards only the molten state. In contrast to assuming neat PPP representing the H3 fraction (20.3 % and 79.7 % solvent) in the ideal dissolution calculation, one has to account for mixed crystal formation. The incorporation of TAGs not being H3 in the mixed crystal cause a reduction of the amount of solvent and, hence, an increase in of the dissolution temperature.

The annealing protocols 2a and 2c appeared to stabilize the mixed crystal formation such that the annealing during heating at 46 °C does not release PPP to recrystallize into *β*. However, the peak at 51.5 °C allows the following interpretation: during annealing, the *β*'-phase packing is rearranged producing a more stable *β*' phase. Since the WAXS pattern does not allow to distinguish two *β*' phases, this argument remains bound to the DSC curve. If a *β* phase is formed due to the release of PPP in 2c, its amount is too little to be captured by WAXS in our experimental setup.

In conclusion, the annealing step introduced in the cooling phase led to a different polymorphic crystallization and mixed crystal formation. When the sample was annealed during cooling, no α phase was observed indicating a direct crystallization into *β*' as the time without supersaturation of an α phase was extended, interfering with the competitive nucleation and growth processes of the different polymorphs. Annealing as means of crystallizing in a directed manner is known from chocolate production, where cocoa butter is tempered in order to generate the nuclei for the formation of the preferred polymorphic form in the product. [51, 52] In shortening production, different temperature-time profiles including annealing procedures can be applied in order to prevent the formation of granular crystal formation in a later stage [38]. Further, annealing during the heating phase revealed a high-melting fraction recrystallizing from a supersaturated solution. Although no β phase was detected in the WAXS pattern, the DSC signal showed one and two high-melting events after 10 and 60 min annealing time, respectively. This suggests the melting of solid PPP or a PPP-rich mixed crystal that emerged after dissolution and recrystallizes in a better packing of higher stability.

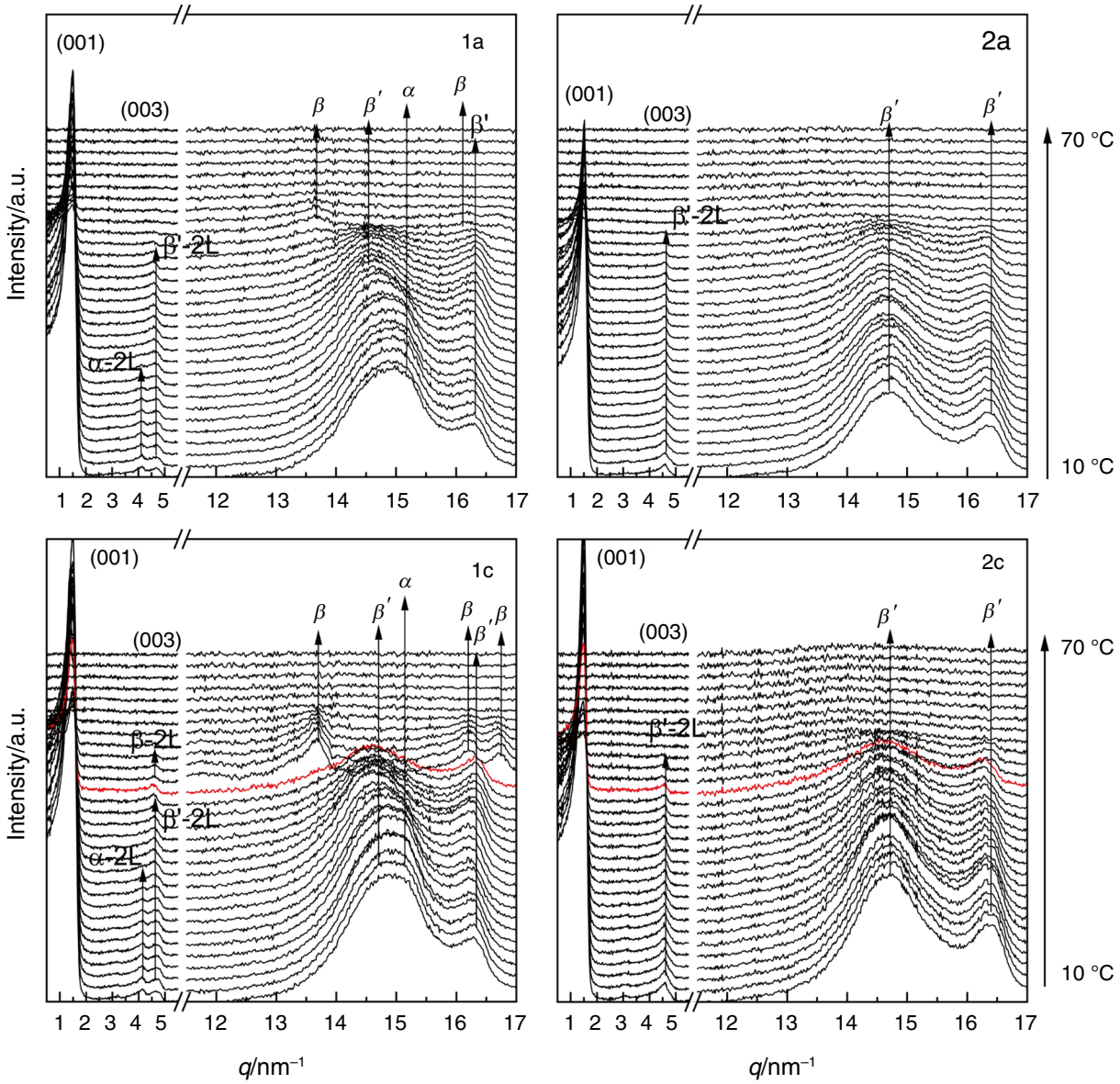

Fig 14 SAXS/WAXS pattern after subtraction of the molten signal (obtained at 70 °C) of PCM obtained during melting at 2 °C min^{-1} undergoing different temperature-time-protocols, 1a, 1c, 2a, and 2c as indicated. Patterns were obtained every 2 °C during the heating. In 1c and 2c, the annealing step was introduced at 46 °C for 60 min. The pattern obtained at 46 °C before annealing is given as red line. Polymorphs are indicated

Conclusions

This study examined four cases in which the recrystallization of high-melting components in PO-based fats was followed by DSC and, in selected cases, time- and temperature-resolved SAXS/WAXS. Different temperature-time profiles including stabilization and annealing procedures were applied to manipulate the crystallization and resulting dissolution pattern.

In Case I, the isothermal crystallization of PO enriched with high-melting saturated TAGs of different origin (FHRO vs. POSt) revealed multiple melting events whose interpretation depended strongly on scan rate. Low scan rates exposed time-dependent recrystallization processes and indicated mixed crystal packing rather than simple polymorphic transitions—an insight supported by complementary SAXS/WAXS. The combination of DSC and SAXS/WAXS allowed a more elaborate interpretation of the melting events as determined alone via DSC for the PO-based blends.

Case II focused on suppressing PPP-recrystallization in PO. Adjusting isothermal stabilization, scan rates, and annealing temperature enabled control over the PPP-rich

α-phase and its recrystallization pathway, yielding comparable DSC curves through different parameter combinations.

In Case III, PPP-driven phase segregation in a PO-based hardstock (PCM) was followed. Different from PO, the PCM also contains TAGs of medium-chain length fatty acids allowing co-crystallization. The melting curves obtained for the PCM spiked with PPP showed the PPP-driven phase segregation during the melting process. The solubility of PPP was estimated via the Hildebrandt equation and aligned reasonably with high-melting peak areas, especially after annealing which improved crystal packing.

Case IV showed that annealing during cooling directs mixed crystal formation in PCM. Annealing suppressed the supersaturation of the α phase and promoted the crystallization of two distinct β' phases, while suppressing PPP-driven melt-induced recrystallization into a β phase. This suggested that via annealing PPP was incorporated in a mixed phase more effectively, which inhibited its release during melting.

Overall, this contribution highlights the need to distinguish true polymorphic transition of a material of fixed composition from recrystallization involving changes of the polymorphic state and composition. Both phenomena can cause phase segregation in multicomponent fat blends. While DSC provides accessible insight into these phenomena, SAXS/WAXS adds structural context. The ability to steer crystallization through tailored temperature-time profiles offers practical leverage for managing co-crystallization in PO-systems and high-melting commercial blends. Future studies should address storage time and temperature cycling effects, which remain unexplored here.

Supplementary Information The online version contains supplementary material available at https://doi.org/10.1007/s10973-026-15468-6.

Author contributions Julia Seilert: Methodology, Investigation, Formal analysis, Visualization, Writing—original draft. Michael Rappolt: Methodology, Writing—review & editing. Georg Dol: Project administration, Funding acquisition, Writing—review & editing. Eckhard Flöter: Supervision, Project administration, Funding acquisition, Writing—review & editing.

Funding Open Access funding enabled and organized by Projekt DEAL.

Data availability Data of this manuscript including SAXS/WAXS data (before liquid subtraction) and DSC data are deposited at Zenodo at https://doi.org/10.5281/zenodo.14879238.

Declarations

Competing interest The authors declare that they have no competing interests.

References

1. Himawan C, Starov VM, Stapley AGF. Thermodynamic and kinetic aspects of fat crystallization. Adv Colloid Interface Sci. 2006;122:3–33. https://doi.org/10.1016/j.cis.2006.06.016.
2. Macridachis-González J, Bayés-García L, Calvet AT. An insight into the solid-state miscibility of triacylglycerol crystals. Molecules. 2020. https://doi.org/10.3390/molecules25194562.
3. Flöter E, Häuptler M, Sato K. Molecular interactions and mixing phase behavior of lipid crystals. In: Sato K, editor. Crystallization of lipids: fundamentals and applications in food, cosmetics, and pharmaceuticals. John Wiley & Sons; 2018. p. 61–104.
4. Sato K, Bayés-García L, Calvet T, Cuevas-Diarte MÀ, Ueno S. External factors affecting polymorphic crystallization of lipids. Eur J Lipid Sci Technol. 2013;115:1224–38. https://doi.org/10.1002/ejlt.201300049.
5. Los J, Flöter E. Construction of kinetic phase diagrams. Phys Chem Chem Phys. 1999. https://doi.org/10.1039/a903245b.
6. Wesdorp LH, van Meeteren J, Jon S, Giessen R, Overbosch P, Grootscholten P, et al. Liquid-multiple solid phase equilibria in fats: theory and experiments. In: Marangoni AG, Wesdorp LH, editors., et al., Structure and properties of fat crystal networks. 2nd ed. Boca Raton: CRC Press; 2013. p. 241–418.
7. Höhne G, Hemminger W, Flammersheim H-J. Differential scanning calorimetry: with 19 tables. 2., revised and enl. ed. Berlin; Heidelberg; New York; Hong Kong; London; Milan; Paris; Tokyo: Springer; 2003.
8. Bayés-García L, Calvet T, Cuevas-Diarte MÀ. Effects of dynamic temperature variations on microstructure and polymorphic behavior of lipid systems. In: Sato K, editor. Crystallization of lipids. Chichester, UK: John Wiley & Sons, Ltd; 2018. p. 183–210. https://doi.org/10.1002/9781118593882.ch6.
9. Busfield WK, Proschogo PN. Thermal analysis of palm stearine by DSC. J Am Oil Chem Soc. 1990;67:171–5.
10. Zhang X, Li L, Xie H, Liang Z, Su J, Liu G, et al. Comparative analysis of thermal behavior, isothermal crystallization kinetics and polymorphism of palm oil fractions. Molecules. 2013;18:1036–52. https://doi.org/10.3390/molecules18011036.
11. Vereecken J, Foubert I, Smith KW, Dewettinck K. Effect of SatSatSat and SatOSat on crystallization of model fat blends. Eur J Lipid Sci Technol. 2009;111:243–58. https://doi.org/10.1002/ejlt.200800150.
12. Vereecken J, Meeussen W, Foubert I, Lesaffer A, Wouters J, Dewettinck K. Comparing the crystallization and polymorphic behaviour of saturated and unsaturated monoglycerides. Food Res Int. 2009;42:1415–25. https://doi.org/10.1016/j.foodres.2009.07.006.
13. Foubert I, Fredrick E, Vereecken J, Sichien M, Dewettinck K. Stop-and-return DSC method to study fat crystallization. Thermochim Acta. 2008. https://doi.org/10.1016/j.tca.2008.02.005.
14. Lutton ES. The polymorphism of tristearin and some of its homologs. J Am Chem Soc. 1945;67:524–7.
15. Small DM. Lateral chain packing in lipids and membranes. J Lipid Res. 1984;25:1490–500.

16. Sato K. Polymorphism of lipid crystals. In: Sato K, editor. Crystallization of lipids: fundamentals and applications in food, cosmetics, and pharmaceuticals. John Wiley & Sons; 2018. p. 17–60.
17. Ollivon M, Bourgaux C, Kalnin D, Villeneuve P, Lesieur P. DSC and high resolutions X-ray diffraction coupling. J Therm Anal Calorim. 2006;85:219–24.
18. Zaliha O, Elina H, Sivaruby K, Norizzah AR, Marangoni AG. Dynamics of polymorphic transformations in palm oil, palm stearin and palm kernel oil characterized by coupled powder XRD-DSC. J Oleo Sci. 2018;67:737–44. https://doi.org/10.5650/jos.ess17168.
19. Calligaris S, Barba L, Arrighetti G, Nicoli MC. Application of DSC-XRD coupled techniques for the evaluation of phase transition in oils and fats and related polymorphic forms. In: Chiavaro E, editor. Differential scanning calorimetry: applications in fat and oil technology. 1st ed. Boca Raton: CRC Press; 2014.
20. Che Man YB, Haryati T, Ghazali HM, Asbi BA. Composition and thermal profile of crude palm oil and its products. J Am Oil Chem Soc. 1999. https://doi.org/10.1007/s11746-999-0224-y.
21. Smith Kevin W. Crystallization of palm oil and its fractions. In: Garti N, editor. Crystallization processes in fats and lipid systems. New York, NY: Dekker; 2001. p. 357–80.
22. Minato A, Ueno S, Yano J, Wang ZH, Seto H, Amemiya Y, et al. Synchrotron radiation X-ray diffraction study on phase behavior of PPP-POP binary mixtures. J Am Oil Chem Soc. 1996;73:1567–72. https://doi.org/10.1007/BF02523526.
23. Kellens M, Meeussen W, Riekel C, Reynaers H. Time resolved X-ray diffraction studies of the polymorphic behaviour of tripalmitin using synchrotron radiation. Chem Phys Lipids. 1990;52:79–98.
24. Kellens M, Meeussen W, Reynaers H. Crystallization and phase transition studies of tripalmitin. Chem Phys Lipids. 1990;55:163–78. https://doi.org/10.1016/0009-3084(90)90077-5.
25. Macridachis J, Bayés-García L, Calvet T. Solid phase behavior of mixture systems based on tripalmitoyl glycerol and monounsaturated triacylglycerols forming a molecular compound. Phys Chem Chem Phys. 2022;24:3749–60. https://doi.org/10.1039/d1cp05361b.
26. Graef V, Dewettinck K, Verbeken D, Foubert I. Rheological behavior of crystallizing Palm oil. Eur J Lipid Sci Technol. 2006;108:864–70. https://doi.org/10.1002/ejlt.200600102.
27. Tangsanthatkun J, Wiking L, Sonwai S, Gregersen SB. Assessment of rheological methods to study crystallization of palm oil fractions. J Texture Stud. 2020;52:169–76. https://doi.org/10.1111/jtxs.12568.
28. Tarabukina E, Jego F, Haudin J-M, Navard P, Peuvrel-Disdier E. Effect of shear on the rheology and crystallization of palm oil. J Food Sci. 2009;74:405–16. https://doi.org/10.1111/j.1750-3841.2009.01304.x.
29. Ng O. A kinetic study on isothermal crystallization of palm oil by solid fat content measurements. J Am Oil Chem Soc. 1994. https://doi.org/10.1007/BF02675908.
30. Mazzanti G, Marangoni AG, Idziak SHJ. Modeling phase transitions during the crystallization of a multicomponent fat under shear. Phys Rev E Stat Phys Plasmas Fluids Relat Interdiscip Topics. 2005. https://doi.org/10.1103/PhysRevE.71.041607.
31. Graef V, van Puyvelde P, Goderis B, Dewettinck K. Influence of shear flow on polymorphic behavior and microstructural development during palm oil crystallization. Eur J Lipid Sci Technol. 2009;111:290–302. https://doi.org/10.1002/ejlt.200800181.
32. Chen CW, Lai OM, Ghazali HM, Chong CL. Isothermal crystallization kinetics of refined palm oil. J Am Oil Chem Soc. 2002;79:403–10. https://doi.org/10.1007/s11746-002-0496-4.
33. Sainlaud C, Taché O, Testard F, Saiter J, Bohin MC, Coquerel G. Impact of cooling profile on refined palm oil crystallization: microscopic and small and wide-angle X-Ray scattering investigations. Eur J Lipid Sci Technol. 2022;124:2100045. https://doi.org/10.1002/ejlt.202100045.
34. West R, Rousseau D. Tripalmitin-driven crystallization of palm oil: the role of shear and dispersed particles. J Am Oil Chem Soc. 2020;97:989–99. https://doi.org/10.1002/aocs.12397.
35. Seilert J, Rappolt M, Dol G, Flöter E. Influence of monounsaturated triglycerides on the crystallization pathway of fully saturated triglycerides. Cryst Growth Des. 2024. https://doi.org/10.1021/acs.cgd.4c01138.
36. Cisneros A, Mazzanti G, Campos R, Marangoni AG. Polymorphic transformation in mixtures of high- and low-melting fractions of milk fat. J Agric Food Chem. 2006;54:6030–3. https://doi.org/10.1021/jf0600814.
37. van Aken GA, Grotenhuis E, van Langevelde AJ, Schenk H. Composition and crystallization of milk fat fractions. J Am Oil Chem Soc. 1999. https://doi.org/10.1007/s11746-999-0146-8.
38. Nguyen V, Rimaux T, Truong V, Dewettinck K, Van Bockstaele F. Granular crystals in palm oil based shortening/margarine: a review. Cryst Growth Des. 2020;20:1363–72.
39. Tanaka L, Tanaka K, Yamato S, Ueno S, Sato K. Microbeam X-ray diffraction study of granular crystals formed in water-in-oil emulsion. Food Biophys. 2009;4:331–9. https://doi.org/10.1007/s11483-009-9131-x.
40. Johansson D, Bergenståhl B. Sintering of fat crystal networks in oil during post-crystallization processes. J Am Oil Chem Soc. 1995;72:911–20. https://doi.org/10.1007/BF02542069.
41. Watanabe A, Tashima I, Matsuzaki N, Kurashige J, Sato K. On the formation of granular crystals in fat blends containing palm oil. J Am Oil Chem Soc. 1992;69:1077–80. https://doi.org/10.1007/BF02541040.
42. Shimomura Y, Tsuchiya M, Ueno S, Shiota M. Effect of triacylglycerol compositions and physical properties on the granular crystal formation of fat blends. J Am Oil Chem Soc. 2019;96:35–42. https://doi.org/10.1002/aocs.12163.
43. Lutton ES. Phase behavior of triglyceride mixtures involving primarily tristearin, 2-oleyldistearin, and triolein. J Am Oil Chem Soc. 1955;32:49–53.
44. Pizzirusso A, Peyronel F, Co ED, Marangoni AG, Milano G. Molecular insights into the eutectic tripalmitin/tristearin binary system. J Am Chem Soc. 2018;140:12405–14. https://doi.org/10.1021/jacs.8b04729.
45. Seilert J, Rappolt M, Dol G, Flöter E. Interplay of polymorphic transition and mixed crystal formation in model fat systems. Cryst Growth Des. 2024;24:1146–58. https://doi.org/10.1021/acs.cgd.3c01164.
46. Kodali D, Atkinson D, Small D. Polymorphic behavior of 1,2-dipalmitoyl-3-lauroyl(PP12)- and 3-myristoyl(PP14)-sn-glycerols. J Lipid Res. 1990;31:1853–64. https://doi.org/10.1016/S0022-2275(20)42329-6.
47. Sato K, Goto M, Yano J, Honda K, Kodali DR, Small DM. Atomic resolution structure analysis of β' polymorph crystal of a triacylglycerol: 1,2-dipalmitoyl-3-myristoyl-sn-glycerol. J Lipid Res. 2001;42:338–45.
48. van Langevelde A, van Malssen KF, Driessen R, Goubitz K, Hollander F, Peschar R, et al. Structure of CnCn+2Cn-type (n = even) beta'-triacylglycerols. Acta Crystallogr B Struct Sci. 2000;B56:1103–11.
49. Lutton ES. Triple chain-length structures of saturated triglycerides. J Am Oil Chem Soc. 1948;70:248–54.
50. Takeuchi M, Ueno S, Sato K. Synchrotron radiation SAXS/WAXS study of polymorph-dependent phase behavior of binary mixtures of saturated monoacid triacylglycerols. Cryst Growth Des. 2003;3:369–74. https://doi.org/10.1021/cg025594r.
51. Ziegler GR. Solidification Processes in Chocolate Confectionery Manufacture. In: Widlak N, Hartel R, Narine S, editors.

Crystallization and Solidification Properties of Lipids. S.l.: AOCS Press; 2001.
52. Schlichter-Aronhime J, Garti N. Solidification and polymorphism in cocoa butter and the blooming problems. In: Garti N, Satō K, editors. Crystallization and polymorphism of fats and fatty acids. New York, N.Y.: Marcel Dekker; 1988.

Authors and Affiliations

Julia Seilert[1] · Michael Rappolt[2] · Georg Dol[3] · Eckhard Flöter[1]

✉ Julia Seilert
julia.seilert@tu-berlin.de

[1] Department of Food Process Engineering, Technische Universität Berlin, Straße des 17. Juni 135, 10623 Berlin, Germany

[2] School of Food Science and Nutrition, University of Leeds, Leeds LS2 9JT, UK

[3] Flora Food Group Research & Development B.V., Food Science Centre, Bronland 18, 6708 WH Wageningen, The Netherlands